A synthetic mechanogenetic gene circuit for autonomous drug delivery in engineered tissues

Robert J. Nims[1,2,3,†], Lara Pferdehirt[1,2,3,4,†], Noelani B. Ho[5,6], Alireza Savadipour[1,2,3,7], Jeremiah Lorentz[1,2,3,4], Sima Sohi[4], Jordan Kassab[4], Alison K. Ross[1,2,3,4], Christopher J. O'Conor[8], Wolfgang B. Liedtke[9], Bo Zhang[3], Amy L. McNulty[5,10], Farshid Guilak[1,2,3,4,7*]

[1] Department of Orthopedic Surgery, Washington University School of Medicine, St. Louis, MO, 63110 USA

[2] Shriners Hospitals for Children - Saint Louis, St. Louis, MO, 63110 USA

[3] Center of Regenerative Medicine, Washington University School of Medicine, St. Louis, MO, 63110

[4] Department of Biomedical Engineering, Washington University, St. Louis, MO 63105

[5] Department of Orthopaedic Surgery, Duke University School of Medicine, Durham, NC 27710

[6] Department of Biology, Duke University, Durham, NC 27708

[7] Department of Mechanical Engineering and Materials Science, Washington University, St. Louis, MO 63105

[8] Department of Pathology and Immunology, Washington University School of Medicine, St. Louis, MO, 63110

[9] Department of Neurology, Duke University School of Medicine, Durham, NC, 27710

[10] Department of Pathology, Duke University School of Medicine, Durham, NC 27710

[†] These authors contributed equally: Robert J. Nims, Lara Pferdehirt

*Corresponding author:

Farshid Guilak, Ph.D.
Professor of Orthopaedic Surgery
Couch Biomedical Research Bldg., Room 3121 Campus Box 8233
Washington University, Saint Louis, MO 63110 Phone: (314) 362-7239
Email: guilak@wustl.edu

Key words:
Synthetic biology, regenerative medicine, gene regulatory network, inflammation, tissue engineering, chondrocyte, cartilage

Running title:
A synthetic mechanogenetic gene circuit

Abstract

Mechanobiologic signals play critical roles in regulating cellular responses under both physiologic and pathologic conditions. Using a combination of synthetic biology and tissue engineering, we developed a mechanically-responsive bioartificial tissue that responds to mechanical loading to produce a pre-programmed therapeutic biologic drug. By deconstructing the signaling networks induced by activation of the mechanically-sensitive ion channel transient receptor potential vanilloid 4 (TRPV4), we created synthetic TRPV4-responsive genetic circuits in chondrocytes. These cells were then engineered into living tissues constructs that respond to mechanical compression to drive the production of the anti-inflammatory biologic interleukin-1 receptor antagonist. Mechanical loading of these tissues constructs in the presence of the cytokine interleukin-1α protected constructs from inflammatory degradation. This "mechanogenetic" approach enables long-term autonomous delivery of therapeutic compounds that are driven by physiologically-relevant mechanical loading with cell-scale mechanical force resolution. The development of synthetic mechanogenetic gene circuits provides a novel approach for the autonomous regulation of cell-based drug delivery systems.

Introduction

Smart biomaterials or bioartificial tissues that autonomously respond to biologic cues and drive a therapeutic or restorative response are promising technologies for treating both chronic and acute diseases (*1*). Mechanotherapeutics in particular, is a rapidly growing class of smart biomaterials that use mechanical signals or mechanical changes within diseased tissues to elicit a therapeutic response (*2-6*) and ameliorate the defective cellular mechanical environment (*7-10*). Current mechanotherapeutic technologies rely on exogeneous protein drug delivery or synthetic polymer implants that offer only a finite lifespan for drug delivery. Creating systems with cellular-scale resolution of mechanical forces that offer long-term, feedback-controlled synthesis of biologic drugs could provide a completely new approach for therapeutic delivery.

In contrast to synthetic polymers, biological tissues grow, adapt, and respond to mechanobiologic signals through the use of specialized molecular components, such as mechanically-sensitive ion channels and receptors that transduce specific stimuli from the physical environment (*11, 12*). In particular, mechanosensitive ion channels are sensitive to both context and deformation mode, making them uniquely suited as mechanotherapeutic sensors (*13-16*). The transient receptor potential (TRP) family is a class of selective ion channels including some mechanically-sensitive members, such as TRPA1, TRPV1, and TRPV4 (*17, 18*). TRPV4 is activated by osmotic fluctuations and plays an important role in the mechanosensitivity of articular cartilage, bladder, uterus, skin, and the dorsal root ganglion (*19-26*). In cartilage, TRPV4 has been shown to regulate the anabolic response of chondrocytes in response to physiologic mechanical strain (*27*).

Osteoarthritis is a chronic cartilage disease for which there are no available disease modifying drugs, ultimately leading to a total joint replacement once the diseased and degraded cartilage and surrounding joint tissues incapacitate a patient from pain and a loss of joint function (*28*). Cartilage tissue engineering is a promising strategy to resurface damaged and diseased articular cartilage with an engineered cartilage tissue construct as a means to reduce the need for, or prolong the time before, a total joint replacement (*29, 30*). An ongoing challenge in the field, however, is developing engineered cartilage constructs that withstand both the high mechanical loads present within the articular joint and the chronic inflammation present within an osteoarthritic joint (*31, 32*). In this regard, a bioartificial tissue that can synthesize biologic drugs in response to inflammation or mechanical loading, either independently or concurrently, could greatly enhance the therapeutic potential of an engineered tissue replacement.

In this study, we engineered a mechanically-responsive bioartificial tissue construct for therapeutic drug delivery by using the signaling pathways downstream of the mechano/osmosensitive ion channel TRPV4 to drive synthetic mechanogenetic gene circuits (Fig. 1). To do this, we first establish that mechanical loading of tissue engineered cartilage activates TRPV4 through fluctuations in the local osmotic environment and not direct mechanical deformation of chondrocytes. We next deconstructed the gene regulatory networks and signaling pathways evoked by TRPV4 activation and revealed the transient activation of several mechanosensitive transcription factors. We engineered synthetic gene circuits to respond to mechanical TRPV4-activation for driving transgene production of an anti-inflammatory biologic interleukin-1 receptor antagonist (IL-1Ra). Lastly, we show that loading engineered cartilage tissue constructs induces an autonomous mechanogenetic response that can protect tissues constructs from an inflammatory insult.

Results

The mechano-osmotic response of chondrocytes to loading is regulated by TRPV4

To deconstruct the mechanotransduction pathways through which chondrocytes perceive mechanical loading, we encapsulated primary porcine chondrocytes within an agarose hydrogel scaffold and loaded these engineered cartilage tissue constructs, while simultaneously imaging the intracellular calcium levels of the chondrocytes. This engineered cartilage system allows for mechanical signals to be transduced to chondrocytes through *de novo* synthesized extracellular matrix in a manner similar to *in vivo* mechanotransduction (*33-35*). Chondrocytes express an array of mechanically-sensitive ion channels and receptors, including TRPV4, Piezo1 and Piezo2, integrins, and primary cilia (*36*), so we investigated the mechanism by which physiologic magnitudes of dynamic mechanical loading are transduced by chondrocytes. Dynamic mechanical loading of engineered cartilage constructs immediately provoked a 108% increase of intracellular calcium response compared with unloaded tissues ($p=0.022$, Fig. 2a). Inhibiting TRPV4 activity using the TRPV4 antagonist GSK205 suppressed load-induced calcium signaling ($p=0.03$), implicating TRPV4 as a critical component in transducing mechanical loading in chondrocytes.

While the molecular structure of TRPV4 has recently been reported (*37*), the mechanisms underlying TRPV4 activation are complex and may involve direct mechanical activation or osmotic activation secondary to mechanical loading of the charged and hydrated extracellular matrix (*17, 19, 38, 39*). To determine the physical mechanisms responsible for TRPV4 activation secondary to tissue compression, we subjected isolated chondrocytes to osmotic loading, direct membrane stretch, and direct single-cell mechanical compression (Fig. 2b, d, e). To better understand the biophysical mechanisms underlying TRPV4 activation, we determined the mechanical state of the chondrocyte membrane in each of these cases using finite element modeling (FEBio; www.febio.org). Chondrocytes rapidly responded to physiologically-relevant changes in media osmolarity through intracellular calcium signals (Fig. 2b). Calcium signaling was highly sensitive to modest changes in osmolarity, with an osmolarity shift of -20 mOsm inducing intracellular signaling in 35% of chondrocytes. All cells were activated by an osmotic shift of -80 mOsm. Inhibition of TRPV4 with GSK205 suppressed calcium signaling during hyposmotic loading (Fig. 2c) similar to the inhibition of TRPV4 activation using the TRPV4 agonist GSK1016790A (GSK101) (Supplemental Fig. S1). Finite element modeling of hyposmotic stress showed that a change of -60 mOsm, sufficient to induce signaling in nearly all chondrocytes, increased cellular volume by 13% and induced an apparent first principle strain of 0.04 homogeneously throughout the membrane (Supplemental Figs. S2 and S3). To investigate the role of direct membrane stretch in TRPV4 activation in the absence of osmotic fluctuations, we used micropipette aspiration of individual chondrocytes to apply controlled deformation of the cell membrane (Fig. 2d). Surprisingly, micropipette aspiration did not provoke any calcium signaling response in chondrocytes, with only 1 of 38 tested cells responding with increased intracellular calcium, indicating that membrane deformation *per se* was not the primary signal responsible for mechanical activation. Finite element simulations of the micropipette experiment showed the presence of heterogenous apparent membrane strains in aspirated chondrocytes, with a first principle strain reaching 0.31 around the micropipette mouth and ~0.04 within the micropipette under an applied pressure of 100 Pa (Supplemental

Fig. S3e-h). To test whether direct calcium signaling in response to mechanical compression of chondrocytes is mediated by TRPV4, we loaded isolated chondrocytes with an atomic force microscope (AFM) to 400 nN (*40*). Only at high, pathologic levels of mechanical compression did direct chondrocyte compression provoke intracellular calcium signaling, and this response was not inhibited by GSK205 (Fig. 2e-g). Finite element modeling predicted an ultimate apparent first principle membrane strain of 2.27 around the cell at the peak cell deformations necessary to elicit intracellular calcium signaling (Supplemental Fig. S3i-l). Together, these findings suggest that activation of TRPV4 in chondrocytes *in situ* may not result directly from cellular strain but rather from osmotic fluctuations induced from the deformation of a chondrocyte's osmotically active environment.

TRPV4 activation in chondrocytes induces transient anabolic and inflammatory signaling networks

We next sought to understand the time course of specific downstream signaling pathways and gene regulatory networks regulated by mechanical activation of TRPV4 using microarray analysis. As TRPV4 is a multimodal channel, downstream signaling is likely dependent on the activation mode, as well as cell and tissue type. To activate TRPV4 in engineered cartilage constructs, we applied either compressive mechanical loading (10% sinusoidal peak-to-peak strain at 1 Hz for 3 h) or pharmacologic stimulation with the TRPV4 agonist GSK101 (1 nM for 3 h) and measured the transcriptional activity at 0, 3, 12, and 20 h following an initial round of stimulation and then at 24 amd 72 h after additional daily bouts of mechanical loading or GSK101 (Fig. 3a). In the 20 h following initial stimulation there were 41 genes upregulated under both mechanical loading and pharmacologic stimulation (Fig. 3b and Supplementary Tables 1 and 2). Upregulation of these targets was immediate and subsided quickly, with transcript levels returning to baseline 12 to 20 h after activation. In particular, the cAMP/Ca^{2+}-responsive transcription factors *C-JUN*, *FOS*, *NR4A2*, and *EGR2* (Fig. 3c) were all upregulated in response to TRPV4-mediated calcium signaling.

We then used Ingenuity Pathway Analysis to identify candidate targets for a synthetic gene circuit that would be responsive to TRPV4 activation. The most significantly enhanced pathway was "the role of osteoblasts, osteoclasts, and chondrocytes in rheumatoid arthritis," with members including transcription factors (*FOS* and *NFATC2*), extracellular matrix synthesis gene (*SPP1*), growth factors (*BMP2* and *BMP6*), and *TNFSF11*, the decoy ligand for RANKL, all of which were upregulated by TRPV4 activation (Fig. 3d). The inflammatory pathways "IL-6 signaling" and "B cell activating factor signaling" were also significantly upregulated by TRPV4 activation, as were the established chondrocyte anabolic pathways "TGF-β signaling" and "Glucocorticoid signaling." Due to the rapid response times of nearly all of the differentially expressed genes, we analyzed which genes responded to repeated bouts of TRPV4 stimulation and found there were 41 genes responsive to mechanical loading and 112 genes responsive to GSK101 supplementation. Of these targets, 15 genes were responsive to both mechanical loading and pharmacologic activation of TRPV4 (Fig. 3e). These targets, the response of which was confirmed by qPCR (Fig. 3f), include both pathways associated with inflammation (*PTGS2*, *SPP1, ATF3*) and cartilage development and homeostasis (*BMP2*, *DUSP5*, *NFATC2*, *INHBA*). Taken together, these data suggest that the TRPV4 mechanotransduction pathway involves activation of a rapidly resolving inflammatory pathway as part of the broad anabolic response to physiologic mechanical loading.

Synthetic mechanogenetic circuits respond to TRPV4 activation to drive transgene expression

TRPV4 activation in response to mechanical loading upregulates a diverse group of targeted genes. Based on the TRPV4-activated signaling pathway (Supplemental Fig. S4), we identified activation of the nuclear factor kappa-light chain enhancer of activated B cells (NF-κB) pathway and upregulation of the prostaglandin-endoperoxidase synthase 2 (*PTGS2*) gene as two distinct avenues to construct TRPV4-responsive synthetic mechanogenetic gene circuits. Targeting the NF-κB signaling pathway and regulation of the *PTGS2* promoter (Fig. 1), we developed two lentiviral systems that would either (1) respond to NF-κB activity by linking 5 synthetic NF-κB binding motifs and a NF-κB negative regulatory element (*41*) with the cytomegalovirus (CMV) enhancer to drive transgene expression of either the therapeutic anti-inflammatory biologic IL-1Ra or a luciferase reporter (henceforth referred to as NFKBr-IL1Ra and NFKBr-Luc, respectively) or (2) respond to *PTGS2* regulation by using a synthetic human *PTGS2* promoter to drive either IL-1Ra or luciferase expression (henceforth referred to as PTGS2r-IL1Ra and PTGS2r-Luc, respectively). We then created mechanogenetically-sensitive engineered cartilage tissue constructs by lentivirally-transducing primary porcine chondrocytes with a mechanogenetic circuit and seeding these cells into an agarose hydrogel to produce synthetically-programmed cartilage constructs (Fig. 4a).

To test whether mechanogenetic tissues actively respond to mechanical stimulation for transgene production, we first applied compressive mechanical loading to NFKBr-IL1Ra-transduced mechanogenetic cartilage constructs, which showed a 38% increase in IL-1Ra production ($p=0.006$) with mechanical loading (Fig. 4b). To establish whether this response was dependent on TRPV4, we antagonized TRPV4 with GSK205 and observed a significant attenuation of NFKBr-IL1Ra circuit activity (Fig. 4b), demonstrating the mechanogenetic circuit responded to both mechanical loading ($p<0.001$) and TRPV4 antagonism ($p<0.001$). Interestingly, GSK205 also reduced circuit activation in unloaded tissues, suggesting TRPV4 activation in chondrocytes may not be entirely dependent on mechanical loading. To further assess the specificity of TRPV4-regulation in mechanogenetic cartilage constructs, we applied hyposmotic loading and pharmacologic GSK101 stimulation to NFKBr-IL1Ra tissues. A step change to hyposmotic media (-200 mOsm change) activated the NFKBr-IL1Ra mechanogenetic circuit ($p=0.019$, Fig. 4c) compared with an isosmotic media change (0 mOsm change). Additionally, daily pharmacologic activation of TRPV4 with 1 nM GSK101 for 3 h d^{-1} over the course of 5 days activated the NFKBr-IL1Ra circuit ($p<0.001$, Fig. 4d). Engineered cartilage constructs responded repeatedly and reproducibly to the daily GSK101 stimulation (Supplemental Fig. S5), demonstrating the role of TRPV4 in activating the mechanogenetic NFKBr-circuits and confirming that a cell-based mechanotherapy can offer prolonged and unabating biologic drug delivery.

To determine the sensitivity and temporal response kinetics of our engineered tissue system, factors critical for the effectiveness of any drug delivery system, we used bioluminescence imaging of NFKBr-Luc or PTGS2r-Luc constructs to determine the dynamic response of mechanogenetic cartilage constructs to TRPV4 activation by mechanical loading or GSK101 pharmacologic stimulation. In response to 10% compressive mechanical loading (Fig. 4e), NFKBr-Luc tissue constructs rapidly peaked (1.8 ± 0.2 h to peak) and decayed ($T_{50\%}$ decay time = 3.4 ± 0.4 h) with loaded samples returning to baseline 4 h after loading. PTGS2r-Luc tissue constructs were slower to activate (21.7 ± 2.7 h to peak) but remained

activated for a longer duration ($T_{50\%}$ decay time = 22.3 ± 1.7 h). This differential in time delivery kinetics may provide strategies by which mechanical loading inputs can drive both short- and long-term drug production by judicious mechanogenetic circuit selection in a single therapeutic tissue construct. To test whether IL-1Ra production followed similar differential production rates, we mechanically loaded NFKBr-IL1Ra and PTGS2r-IL1Ra tissues constructs and measured protein levels of IL-1Ra released in the media. One round of mechanical loading activated NFKBr-IL1Ra tissues by 24 h, as measured by an increase in IL-1Ra produced in the loaded tissue constructs. This differential in IL-1Ra concentration between loaded and free swelling constructs remained constant at 72 h, indicating loaded mechanogenetic tissues resumed baseline activity after 24 hours (Fig. 4f). Conversely, a single round of mechanical loading activated PTGS2r-IL1Ra tissues to produce more IL-1Ra after 48 h compared to free swelling tissues, and the IL-1Ra difference between loaded and free swelling tissues continued to increase by 72 h. This confirmed that loaded PTGS2r-tissue constructs remained activated up to 72 h after loading and demonstrated a longer-acting mechanogenetic response in the PTGS2r-system (Fig. 4g). These results show that complex drug delivery strategies can be programmed into a single mechanogenetic tissue constructs to produce multiple modes and time-scales of therapeutic or regenerative biologic drug delivery.

For insight into the dose-response relationship and sensitivity of the mechanogenetic gene circuits, we imaged NFKBr-Luc and PTGS2r-Luc bioluminescence in response to different doses of GSK101. Temporal imaging revealed that GSK101 stimulation produced similar rise and decay kinetics as TRPV4-activation from mechanical loading (Fig. 4e) in NFKBr-Luc (Fig. 4h) and PTGS2r-Luc (Fig. 4i) cartilage tissue constructs. Both mechanogenetic tissues constructs displayed a clear dose-dependent activation from GSK101 stimulation as demonstrated by the AUC. NFKBr-Luc tissue constructs were responsive from 1 through 9 nM GSK101, whereas PTGSr-Luc tissue constructs plateaued in responsiveness at 6 nM GSK101 (Fig. 4i). Based on this pharmacologic sensitivity, we hypothesized mechanogenetic constructs would be increasingly activated by higher mechanical loading strains through increased osmotic stimulation (Fig. 2b). As NFKBr-Luc tissues demonstrated the most pronounced GSK101 dose-dependent response, we applied dynamic compressive strain amplitudes from 0 to 15% to NFKBr-IL1Ra tissue constructs to span the range of physiologic strains expected for articular cartilage *in vivo* (*33*). We measured elevated production of IL-1Ra with increasing compressive strains (Fig. 4j; slope = 8 ± 2 ng/g IL-1Ra/%strain, $p<0.001$), demonstrating that drug production is directly responsive to the magnitude of mechanical loading in our mechanogenetic engineered tissues.

Mechanical activation of the mechanogenetic engineered cartilage protects cartilage explants from IL-1α-induced inflammation-driven degradation

The long-term success of engineered cartilage implants depends on the ability of implants to withstand the extreme loading and inflammatory stresses within an injured or osteoarthritic joint (*42*). We hypothesized that loading would activate mechanogenetic tissues constructs to produce therapeutic levels of IL-1Ra and protect engineered cartilage constructs and the surrounding joint from destructive inflammatory cytokines. As our mechanogenetic circuits rely on signaling pathways that overlap with the cellular inflammatory response, we examined the dose-response of IL-1Ra production in response to the inflammatory cytokine interleukin-1α (IL-1α; Figs. 5a and c). NFKBr-IL1Ra

mechanogenetic constructs responded to exogeneous IL-1α supplementation following a dose-dependent characteristic, consistent with findings of IL-1-induced NF-κB signaling in chondrocytes ((*43*), Fig. 5b). Importantly, this dose-dependent response to IL-1α was present up to 10 ng/mL and offered prolonged and robust production of IL-1Ra, promoting the notion that cell-based tissues may offer a more sustained ability to produce therapeutic biomolecules relative to traditional acellular approaches (Supplementary Fig. S6). Mechanical loading further enhanced IL-1Ra production in the presence of IL-1α, demonstrating that even in the presence of high levels of inflammation, mechanical loading further potentiates NF-κB signaling (Supplementary Fig. S7). Interestingly mechanogenetic PTGS2r-IL1Ra and PTGS2r-Luc constructs demonstrated no sensitivity to IL-1α (Figs. 5d and e). Importantly, and in contrast to NFKBr-tissues constructs, the selective sensitivity to TRPV4 activation and not to IL-1α in PTGS2r-tissue constructs suggests that this system is distinctively mechanically-sensitive. This distinction was further demonstrated in tissues exposed to both IL-1α inflammation and osmotic loading, wherein only loading played a significant influence (Supplemental Fig. S8, $p=0.0002$ for loading and $p=0.14$ for inflammation).

To test whether loading-induced IL-1Ra production would protect engineered mechanogenetic tissue constructs against IL-1α, we co-cultured mature, 21-days-old NFKBr-tissue constructs with articular cartilage explants in the presence of IL-1α inflammation and daily hyposmotic loading to model the inflammation and loading conditions present in arthritic joints (Figs. 5f and j). Using NFKBr-Luc tissue constructs, which lack an anti-inflammatory response to loading and IL-1α (Fig. 5g), to simulate how conventional engineered cartilage constructs would respond in an arthritic joint, constructs lost 45.6% of their sulfated-glycosaminoglycan content (Fig. 5h, S-GAG). S-GAGs are essential structural molecules that impart mechanical integrity and strength in both engineered and native cartilage (*44, 45*). Osmotic loading did not modulate this response and the substantial S-GAG loss was observable histologically through diminished safranin-O staining throughout the tissue (Fig 5i). In the anti-inflammatory NFKBr-IL1Ra tissues constructs, osmotic loading in the presence of inflammatory IL-1α increased IL-1Ra production 93% over isosmotic control tissues also cultured with IL-1α (Fig. 5j). After 72 h of treatment, IL-1α induced a 30.8% loss of S-GAG in NFKBr-IL1Ra engineered cartilage constructs under isosmotic conditions, while NFKBr-IL1Ra engineered cartilage that was incubated with IL-1α and osmotically loaded did not significantly lose their S-GAG content (Fig. 5l). Histologically, hyposmotic loading NFKBr-IL1Ra engineered cartilage constructs maintained rich safranin-O staining of S-GAG throughout the constructs, even in the presence of IL-1α (Fig. 5m). Together these data demonstrate engineered mechanogenetic cartilage constructs can produce anti-inflammatory IL-1Ra in response to osmotic loading at levels sufficient for engineered tissue protection in a proinflammatory environment mimicking the conditions present in an osteoarthritic joint (*46*).

Discussion

By combining synthetic biology and tissue engineering, we developed a novel class of bioartificial material that is mechanogenetically-sensitive. This system functions by redirecting endogenous mechanically-sensitive ion channels to drive synthetic genetic circuits for converting mechanical inputs into programmed expression of a therapeutic transgene.

By engineering these cells into a functional tissue construct, this system provides the potential to repair or resurface damaged cartilage, while providing site-specific, mechanically-induced anti-cytokine therapy against inflammation. Our approach is based on redirection of the downstream response to activation of the TRPV4 ion channel – a critical mechanosensor in cartilage – to transduce tissue-scale deformational mechanical loading via mechano-osmotic coupling in the charged extracellular matrix. By deconstructing the gene regulatory networks activated by mechanically-induced TRPV4, we co-opted chondrocyte-endogenous signaling machinery to drive synthetic circuits for the production of therapeutic biologic drugs, using the anti-inflammatory drug IL-1Ra as a model system for proof of concept. Our results also demonstrate the use of distinct signaling networks for defining the specificity, timing, and dose-response for the expression of therapeutic biologic drugs. We show that a single round of mechanical loading can induce short-term and long-term responses based on the particular response of the synthetic circuit. While we targeted a treatment for cartilage repair and osteoarthritis, pathologic mechanical loading and mechanosignaling play a role in a broad range of acute and chronic diseases (*11*), suggesting a wide range of potential therapeutic applications for mechanogenetically regulated cells or tissues requiring autonomous cellular control systems.

While we developed mechanogenetic cartilage tissues based on TRPV4-activation here, the use of other native, mechanically-sensitive ion channels and receptors is an attractive source of mechanosensors that can be elicited to provoke synthetic outputs. Expanding mechanogenetic approaches to additional mechanosensors and tissues would increase the range of physical stimuli that synthetic circuits can respond to, but requires an in-depth understanding of both the mechanical contexts necessary for mechanosensor activation and the resulting downstream signaling pathways. The fact that primary chondrocytes possess an array of different mechanically-sensitive ion channels and receptors highlights the potential opportunities to layer mechanosensor-specific circuits and produce systems responsive to different mechanical inputs that drive specific synthetic outputs. Our analysis here demonstrates that physiologic (~10%, 1 Hz) mechanical loading of engineered cartilage is converted to a mechano-osmotic signal that activates TRPV4. To this end, we examined the mechanoresponsiveness of TRPV4 signaling and developed two genetic circuits that respond to TRPV4 activation. The use of alternate chondrocyte mechanosensors remains an attractive area of research. For instance, the lack of a TRPV4-dependent response to high AFM loads is consistent with our earlier finding that high, potentially injurious, cellular strains are transduced via the Piezo family of ion channels (*40*). The multimodal nature of TRPV4, and the TRP family more generally (*47*), suggests additional genetic circuits may be developed for alternate activation modes by characterizing the downstream signaling networks that respond to temperature or biochemical activation of the channel (*48*). Moreover, engineering novel mechanosensors may open the opportunity for developing custom mechanical activation modes and orthogonal downstream signaling in future mechanogenetic systems.

Our findings offer a detailed perspective of the complex cellular events initiated by TRPV4 activation in chondrocytes. TRPV4 has been thought to play a largely anabolic role in chondrocytes through enhanced synthesis of matrix molecules, S-GAG and collagen, and upregulation of TGF-β3 (*27*), which is evident in our GO/KEGG pathways hits of "TGF-β Signaling" and "Glucocorticoid Receptor Signaling". However, our findings also revealed the presence of an acute, transient resolving inflammatory response (pathways including "Chondrocytes in RA," "IL-6 Signaling," "April Mediated Signaling," and "B Cell Activating Factor Signaling"). These findings are particularly striking as the physiologic levels of

mechanical loading applied here (10% compressive strain) are typically associated with promoting chondrocyte anabolism (*27*), although our data is in line with other reports suggesting a proinflammatory role of TRPV4 (*21, 49, 50*). Together, the rapidly-resolving mechanical load-induced inflammation in this context may be part of a natural cascade by which a quickly-decaying inflammatory response is characteristic of the regenerative, anabolic response to mechanical loading (*51, 52*). Additionally, increasing evidence suggests a potential role for TRPV4 in mediating cellular and tissue inflammation, and studies of chondrocyte-specific TRPV4-knockout mice report a decreased severity of age-associated OA (*49*). A load-induced mechanism of chondrocyte inflammation through TRPV4 may be a future target of age-associated OA and other age-associated diseases (*21, 50, 53*). Our circuits here highlight the opportunities to target different responses through downstream pathway selection, namely using an NFKBr-circuit that is sensitive to IL-1α inflammation and a PTGS2r-circuit that is IL-1α-insensitive.

Using an engineered, living tissue construct for coordinated drug delivery obviates many of the traditional limitations of "smart" materials, such as long-term integration, rapid dynamic responses, and extended drug delivery without the need for replacement or reimplantation of the drug delivery system. The modular approach of using cells as both the mechanosensors and the effectors within engineered tissues allows for regulation and sensitivity at the mechanically-sensitive channel or receptor level, the signaling network level, and the gene circuit level. While we used the primary chondrocyte's endogenous TRPV4 to drive our synthetic system, engineering novel mechanically-sensitive proteins may beckon a new frontier for coordinating inputs or driving receptor activation from novel and precise mechanical inputs. Together, this framework for developing mechanically-responsive engineered tissues is a novel approach for establishing new autonomous therapeutics and drug delivery systems for mechanotherapeutics.

Materials and Methods

Tissue harvest, cell isolation, agarose gel casting, and culture

Full-thickness porcine articular chondrocytes were enzymatically isolated from the femurs of pigs (~30 kg; 12-16 weeks old) using collagenase (Sigma) media. Filtered cells were mixed 1:1 with 4% molten type VII agarose (Sigma) and the cells-agarose mixture was injected into a gel apparatus and allowed to set at room temperature. Chondrocyte-laden disks were punched out yielding engineered cartilage at a final concentration of 2% agarose and 15-20 million cells/mL. All constructs were given 2-3 d to equilibrate and media were changed three times per week during chondrogenic culture using a base media of DMEM-High Glucose (Gibco) supplemented with 10% FBS (Atlas), 0.1 mM nonessential amino acids (Gibco), 15 mM HEPES (Gibco), 40 µg/mL proline (Sigma), 1x-penicillin, streptomycin, and fungizone (Gibco), and fresh 50 µg/mL ascorbyl-2-phosphate (Sigma) and maintained at 37°C and 5% CO_2 (*54*).

Chondrocyte mechanical and pharmacologic stimulation

Confocal imaging of mechanical compression

A custom mechanical compression device was used to compress agarose constructs while simultaneously performing intracellular calcium imaging on a confocal microscope (Zeiss LSM880) using fluo-4 AM and fura-red AM (ThermoFisher Scientific) based on manufacturer's protocols. Opposing platens were controlled with stepper motors to apply 60 rounds of compressive loading (10%) after a 2% tare strain. Ratiometric calcium imaging (Calcium Ratio = $\text{Intensity}_{\text{fluo-4}}/\text{Intensity}_{\text{fura-red}}$) was analyzed within each sample with ImageJ before and after the mechanical loading.

High-throughput mechanical compression

A custom mechanical compression device was used for sinusoidal compression of 24-individual tissue constructs simultaneously (*54*) using a closed loop displacement-feedback system. This system allows for compression at 37 C and 5% CO_2.

Osmotic stimulation

For calcium-imaging studies, osmotic loading media were prepared using HBSS media (Gibco). For mechanogenetic-tissue culture studies, osmotic loading media were prepared using ITS+ DMEM media. These media were titrated to hypoosmotic media by adding distilled water and measured with a freezing-point osmometer (Osmette 2007; Precision Systems). For osmotic stimulation of mechanogenetic samples, standard culture media (containing 10% FBS) was replaced with isosmotic (380 mOsm) ITS+ base media 3 d before osmotic loading to acclimate tissues.

Micropipette aspiration

Detail methods for micropipette aspiration are described in Trickey et al, 2006 (*55*). Briefly, glass micropipettes were drawn to a diameter of ~10 µm and coated with Sigmacote (Sigma) to prevent cell binding to the glass micropipette. The micropipette was brought in contact with a cell, and a tare pressure of 10 Pa was applied for a period of 3 minutes. Increasing step pressures were then applied in increments of 100 Pa were then applied for 3 minutes each until the cell was fully aspirated. Laser scanning microscopy was used to measure cell deformation (DIC channel) and $[Ca^{2+}]_i$ throughout the experiment. Ratiometric calcium imaging, as described above, was performed to assess the mechanoresponse of chondrocytes to micropipette aspiration, however we found the application of step increases in pressure to the cell surface using a micropipette rarely initiated a Ca^{2+} transient.

Atomic Force Microscopy

Freshly isolated chondrocytes were plated on glass coverslips and incubated for 2-3 d. Prior to atomic force microscopy (AFM) compression, cells were incubated with 10 µM GSK205 or DMSO (vehicle) and stained with intracellular calcium dye Fura-2 AM (Molecular Probes) according to manufacturer's protocols. Cells were loaded to 400 nN using a AFM (Asylum Research MFP-3D) with tipless cantilevers (k=6.2 N/m; MikroMasch) while simultaneously recording intracellular calcium levels with an Olympus microscope and cycled with 340 nm and 380 nm light to produce a ratiometric output (Calcium Ratio = $\text{Intensity}_{\text{Fura-2 @ 380 nm}} / \text{Intensity}_{\text{Fura-2 @ 340 nm}}$) for intracellular calcium levels which were analyzed with ImageJ (*40*).

Pharmacologic TRPV4 modulation

GSK1016790A (GSK101, Millipore-Sigma) was resuspend at final concentrations (1-10 nM) and matched with a DMSO (vehicle) control. GSK205 (manufactured at the Duke Small Molecule Synthesis facility) was used as a TRPV4-specific inhibitor and pre-incubated with samples before analysis to allow for diffusion within three-dimensional tissues and used at a final concentration of 10 μM with appropriate DMSO (vehicle) controls.

FLIPR assay

After digestion and isolation, filtered chondrocytes were plated in a 96-well plate at 10,000 cells per well and left for 24 hours before stimulation on a fluorescent imaging plate reader (FLIPR) by which individual wells were stimulated with either osmotic or GSK101-containing media. Cellular response in each well was measured via fluo-4 intracellular calcium dye using the fluo-4 NW calcium assay kit (Molecular Probes) according to manufacturer's directions. GSK205 was pre-incubated and added alongside stimulated and unstimulated chondrocytes to directly assess the TRPV4-dependent response of osmotic and pharmacologic stimulation.

Finite element modeling

Finite element models of cellular deformation were performed using the FEBio (www.febio.org) finite element software package (version 2.6.4). Models were run using a Neo-Hookean elastic material for the cell and membrane compartments of the cell (*56*). All model geometries utilize axisymmetry boundary conditions to reduce the model size. Osmotic loading was assessed using a Donnan osmotic loading material with parameters taken from the van't Hoff relation for chondrocytes under osmotic loading and loading chondrocytes with a -60 mOsm osmotic media shift. Models for micropipette aspiration were run assuming a cell modulus of 1 kPa and Poissons ratio of 0.4 while imposing a pressure of -200 Pa to the cell (*55*). Models of single-cell direct deformational loading (AFM) were performed by simulating an elastic sphere being compressed to 13% of its original height.

Microarray collection and analysis

After a 14 d preculture, engineered cartilage constructs (∅4 mm × 2.25 mm) were stimulated under 10% compressive loading or 1 nM GSK101 for 3 h d^{-1} for 3 d. An unstimulated control (free-swelling) was cultured under identical conditions. Immediately after stimulation, constructs were washed and then fed with culture media. Constructs were snap frozen in liquid N_2 at 0, 3, 6, 12, 20, 24, and 72 hours after initial stimulation. Total RNA was extracted from the constructs using a pestle homogenizer and the Norgen Biotek RNA/protein purification plus kit. RNA quantity and quality were assessed by Nanodrop (Thermoscientific) and the Agilent Bioanalyzer. Total RNA was processed using the Ambion WT expression labeling kit and the Porcine Gene 1.0 ST Array (Affymetrix). The raw-signal of arrays were induced into R environment and quantile-normalized by using *'affy'* and *'oligo'* package. The significantly differentially expressed genes (DEGs) were identified and analyzed by using one regression model in R with package *'genefilter'*, *'limma'*, *'RUV'*, *'splines'*, *'gplots'* and *'plotly'* at adjusted p-value cutoff 0.05. Then the DEGs were

imported into Ingenuity Pathway Analysis (IPA) to perform the pathway enrichment analysis. The DEG heatmap was plotted by using *'gplots'* in R.

Mechanogenetic circuit design, development, viral development, and culture

We developed two lentiviral systems consisting of an NF-κB inducible promoter upstream of either IL-1Ra (NFKBr-IL1Ra) or luciferase (NFKBr-Luc). Therefore, upon NF-κB signaling, either IL-1Ra (NFKBr -IL1Ra) or luciferase (NFKBr -Luc) is expressed as a measure of mechanogenetic circuit activation. Additionally, we developed two lentiviral systems consisting of a synthetic human *PTGS2* promoter upstream of either IL-1Ra (PTGS2r-IL1Ra) or luciferase (PTGS2r-Luc). Therefore, when *PTGS2* is activated either IL-1Ra or luciferase is expressed.

NFKBr-circuit design

A synthetic NF-κB inducible promoter was designed to incorporate multiple NF-κB response elements (*41*). A synthetic promoter was developed containing five consensus sequences approximating the NF-κB canonical recognition motif based on genes upregulated through inflammatory challenge: *InfB1, Il6, Mcp1, Adamts5,* and *Cxcl10* (*57*). A TATA box derived from the minimal CMV promoter was cloned between the synthetic promoter and downstream target genes, either murine *Il1rn* or firefly luciferase from the pGL3 basic plasmid (Promega), and an NF-κB-negative regulatory element (NRE-5'-AATTCCTCTGA-3') was cloned upstream of the promoter to reduce background signal (*58*).

PTGS2r-circuit design

A synthetic human *PTGS2* promoter was obtained from SwitchGear Genomics and cloned into the NFKBr-IL1Ra or NFKBr-Luc lentiviral transfer vectors in place of the NF-κB inducible promoter using Gibson Assembly to create the PTGS2r-IL1Ra and PTGS2r-Luc circuits (*59*).

Lentivirus production

HEK293T were co-transfected with second-generation packaging plasmid psPAX2 (No. 12260; Addgene), an envelope plasmid pMD2.G (No. 12259; Addgene), and the expression transfer vector by calcium phosphate precipitation to make vesicular stomatitis virus glycoprotein pseudotyped lentivirus (LV) (*60*). The lentivirus was stored at -80℃until use. The expression transfer vectors include the NFKBr-IL1Ra, NFKBr-Luc, PTGS2r-IL1Ra, and PTGS2r-Luc plasmids. The functional titer of the virus was determined with quantitative real-time polymerase chain reaction to determine the number of lentiviral DNA copies integrated into the genome of transduced HeLa cells (*60*).

Mechanogenetic circuit testing outcome measures

Assessing mechanogenetic tissue construct activation in IL-1Ra producing constructs was measured with an enzyme linked immunosorbent assay (ELISA) for mouse IL-1Ra (R&D Biosystems) according to manufacturer's protocols. Data are reported as the amount of IL-1Ra produced per construct (in ng) normalized by the tissue wet weight mass of the construct (in g). Luciferase-based mechanogenetic protection was assessed using a bioluminescent imaging reader

(Cytation5, BioTek) at 37 °C and 5% CO2 and cultured in phenol-red free high-glucose DMEM supplemented with 1% ITS+, 2 mM Glutamax, 1 mM sodium pyruvate, 15 mM HEPES, 40 µg/mL proline, 1x-penicillin/streptomycin, and 1 µM luciferin. Prior to stimulation, samples were imaged under free-swelling conditions for ~1 d to get a baseline bioluminescent level (F_o). For mechanical loading studies, constructs were then mechanically loaded or similarly transferred for a free-swelling control and then returned to the bioluminescent imaging. For GSK101 pharmacologic studies, the bioluminescent media (above) was supplemented with GSK101 or DMSO (vehicle control) to the appropriate dose (1-10 nM) and simultaneously imaged for 3 h, before washing and replacing with standard bioluminescent media. Pre-stimulation baseline was normalized from post-stimulation bioluminescent readings (F) to yield F/F_o as the outcome measure.

Coculture studies

To assess mechanogenetic anti-inflammatory protection, NFKBr-IL1Ra constructs were cultured with a porcine cartilage explant for 72 h in the presence of 0 or 0.1 ng/mL porcine IL-1α. Porcine cartilage explants (3 mm diameter) were cored from condyle cartilage and the subchondral bone was removed, leaving a cartilage explant ~1-2 mm thick including the superficial, middle, and deep zones and cultured in isosmotic ITS+ base media until experimentation. Mechanical loading was applied daily with 3 h/d hypoosmotic loading (180 mOsm) before returning to the isosmotic media (380 mOsm) containing the explant and IL-1α. Isosmotic controls were moved similarly to an isosmotic media (380 mOsm). Control, non-anti-inflammatory mechanogenetic tissue constructs, consisted of NFKBr-Luc tissues. Tissue sulfated glycosaminoglycan proteoglycans (S-GAG) content in the engineered tissue construct and media were assessed with the DMB assay (*61*). Tissue samples were digested with papain overnight (60 °C) to measure tissue S-GAG using the DMB assay. Bulk S-GAG amount was normalized to tissue wet weight. Constructs were fixed in neutral buffered formalin overnight before embedding in paraffin and sectioning to 7 µm. Histological slices were stained with safranin-O to examine S-GAG distribution and abundance.

Statistical analysis

Data were analyzed with one-way ANOVA or two-way ANOVA (α=0.05) where appropriate using R software (www.r-project.org). For two-way ANOVAs, individual groups were compared using a Tukey post-hoc analysis when the interaction of factors was also significant. Correlation trends of strain magnitude to IL-1Ra production was analyzed in R using linear model analysis. Temporal bioluminescent data were analyzed using a two-tailed t-test comparison between the groups at each analyzed time point.

References

1. Y. Lu, A. A. Aimetti, R. Langer, Z. Gu, Bioresponsive materials. *Nature Reviews Materials* **2**, 16075 (2017).

2. A. M. Gerdes, J. M. Capasso, Structural remodeling and mechanical dysfunction of cardiac myocytes in heart failure. *J. Mol. Cell. Cardiol.* **27**, 849-856 (1995).

3. H. D. Intengan, E. L. Schiffrin, Structure and mechanical properties of resistance arteries in hypertension: role of adhesion molecules and extracellular matrix determinants. *Hypertension* **36**, 312-318 (2000).

4. D. F. Meaney, D. H. Smith, Biomechanics of concussion. *Clin. Sports Med.* **30**, 19-31 (2011).

5. M. Plodinec *et al.*, The nanomechanical signature of breast cancer. *Nature nanotechnology* **7**, 757 (2012).

6. D. D. Anderson *et al.*, Post- traumatic osteoarthritis: improved understanding and opportunities for early intervention. *J. Orthop. Res.* **29**, 802-809 (2011).

7. K. Y. Lee, M. C. Peters, K. W. Anderson, D. J. Mooney, Controlled growth factor release from synthetic extracellular matrices. *Nature* **408**, 998 (2000).

8. M. B. Larsen, A. J. Boydston, Successive mechanochemical activation and small molecule release in an elastomeric material. *J. Am. Chem. Soc.* **136**, 1276-1279 (2014).

9. D. Mertz *et al.*, Mechanotransductive surfaces for reversible biocatalysis activation. *Nature materials* **8**, 731 (2009).

10. J. Wang, J. A. Kaplan, Y. L. Colson, M. W. Grinstaff, Mechanoresponsive materials for drug delivery: Harnessing forces for controlled release. *Advanced drug delivery reviews* **108**, 68-82 (2017).

11. D. Ingber, Mechanobiology and diseases of mechanotransduction. *Ann. Med.* **35**, 564-577 (2003).

12. C. T. Lim, A. Bershadsky, M. P. Sheetz. (The Royal Society, 2010).

13. J. Wu, A. H. Lewis, J. Grandl, Touch, tension, and transduction–the function and regulation of Piezo ion channels. *Trends Biochem. Sci.* **42**, 57-71 (2017).

14. R. P. Seal *et al.*, Injury-induced mechanical hypersensitivity requires C-low threshold mechanoreceptors. *Nature* **462**, 651 (2009).

15. W. Lee, F. Guilak, W. Liedtke, in *Current topics in membranes*. (Elsevier, 2017), vol. 79, pp. 263-273.

16. S. S. Ranade, R. Syeda, A. Patapoutian, Mechanically activated ion channels. *Neuron* **87**, 1162-1179 (2015).

17. A. P. Christensen, D. P. Corey, TRP channels in mechanosensation: direct or indirect activation? *Nature Reviews Neuroscience* **8**, 510 (2007).

18. C. Moore, R. Gupta, S. E. Jordt, Y. Chen, W. B. Liedtke, Regulation of Pain and Itch by TRP Channels. *Neurosci. Bull.* **34**, 120-142 (2018).

19. M. N. Phan *et al.*, Functional characterization of TRPV4 as an osmotically sensitive ion channel in porcine articular chondrocytes. *Arthritis & Rheumatism: Official Journal of the American College of Rheumatology* **60**, 3028-3037 (2009).

20. T. Gevaert *et al.*, Deletion of the transient receptor potential cation channel TRPV4 impairs murine bladder voiding. *The Journal of clinical investigation* **117**, 3453-3462 (2007).

21. L. Ying *et al.*, The transient receptor potential vanilloid 4 channel modulates uterine tone during pregnancy. *Sci. Transl. Med.* **7**, 319ra204-319ra204 (2015).

22. M. Suzuki *et al.*, Localization of mechanosensitive channel TRPV4 in mouse skin. *Neurosci. Lett.* **353**, 189-192 (2003).

23. M. Suzuki, A. Mizuno, K. Kodaira, M. Imai, Impaired pressure sensation in mice lacking TRPV4. *J. Biol. Chem.* **278**, 22664-22668 (2003).

24. W. Liedtke *et al.*, Vanilloid receptor-related osmotically activated channel (VR-OAC), a candidate vertebrate osmoreceptor. *Cell* **103**, 525-535 (2000).

25. W. Liedtke, D. M. Tobin, C. I. Bargmann, J. M. Friedman, Mammalian TRPV4 (VR-OAC) directs behavioral responses to osmotic and mechanical stimuli in Caenorhabditis elegans. *Proceedings of the National Academy of Sciences* **100**, 14531-14536 (2003).

26. W. Liedtke, J. M. Friedman, Abnormal osmotic regulation in trpv4-/- mice. *Proc. Natl. Acad. Sci. U. S. A.* **100**, 13698-13703 (2003).

27. C. J. O'Conor, H. A. Leddy, H. C. Benefield, W. B. Liedtke, F. Guilak, TRPV4-mediated mechanotransduction regulates the metabolic response of chondrocytes to dynamic loading. *Proceedings of the National Academy of Sciences* **111**, 1316-1321 (2014).

28. D. T. Felson *et al.*, Osteoarthritis: new insights. Part 2: treatment approaches. *Ann. Intern. Med.* **133**, 726-737 (2000).

29. A. D. Cigan *et al.*, Nutrient channels aid the growth of articular surface-sized engineered cartilage constructs. *Tissue Engineering Part A* **22**, 1063-1074 (2016).

30. F. T. Moutos *et al.*, Anatomically shaped tissue-engineered cartilage with tunable and inducible anticytokine delivery for biological joint resurfacing. *Proc. Natl. Acad. Sci. U. S. A.* **113**, E4513-4522 (2016).

31. P. H. Ousema *et al.*, The inhibition by interleukin 1 of MSC chondrogenesis and the development of biomechanical properties in biomimetic 3D woven PCL scaffolds. *Biomaterials* **33**, 8967-8974 (2012).

32. R. J. Nims *et al.*, (*) Constrained Cage Culture Improves Engineered Cartilage Functional Properties by Enhancing Collagen Network Stability. *Tissue Eng Part A* **23**, 847-858 (2017).

33. J. Sanchez-Adams, H. A. Leddy, A. L. McNulty, C. J. O'Conor, F. Guilak, The mechanobiology of articular cartilage: bearing the burden of osteoarthritis. *Curr. Rheumatol. Rep.* **16**, 451 (2014).

34. R. L. Mauck *et al.*, Functional tissue engineering of articular cartilage through dynamic loading of chondrocyte-seeded agarose gels. *J. Biomech. Eng.* **122**, 252-260 (2000).

35. D. A. Lee, T. Noguchi, S. P. Frean, P. Lees, D. L. Bader, The influence of mechanical loading on isolated chondrocytes seeded in agarose constructs. *Biorheology* **37**, 149-161 (2000).

36. F. Guilak, R. J. Nims, A. Dicks, C.-L. Wu, I. Meulenbelt, Osteoarthritis as a disease of the cartilage pericellular matrix. *Matrix Biol.* **71**, 40-50 (2018).

37. Z. Deng *et al.*, Cryo-EM and X-ray structures of TRPV4 reveal insight into ion permeation and gating mechanisms. *Nat. Struct. Mol. Biol.* **25**, 252 (2018).

38. S. Loukin, X. Zhou, Z. Su, Y. Saimi, C. Kung, Wild-type and brachyolmia-causing mutant TRPV4 channels respond directly to stretch force. *J. Biol. Chem.* **285**, 27176-27181 (2010).

39. M. R. Servin-Vences, M. Moroni, G. R. Lewin, K. Poole, Direct measurement of TRPV4 and PIEZO1 activity reveals multiple mechanotransduction pathways in chondrocytes. *Elife* **6**, e21074 (2017).

40. W. Lee *et al.*, Synergy between Piezo1 and Piezo2 channels confers high-strain mechanosensitivity to articular cartilage. *Proceedings of the National Academy of Sciences* **111**, E5114-E5122 (2014).

41. L. Pferdehirt, A. K. Ross, J. M. Brunger, F. Guilak, A Synthetic Gene Circuit for Self-Regulating Delivery of Biologic Drugs in Engineered Tissues. *Tissue Engineering Part A* **25**, 809-820 (2019).

42. K. W. Ng *et al.*, Passaged adult chondrocytes can form engineered cartilage with functional mechanical properties: a canine model. *Tissue Engineering Part A* **16**, 1041-1051 (2009).

43. T. Chowdhury, D. Salter, D. Bader, D. Lee, Signal transduction pathways involving p38 MAPK, JNK, NFκB and AP-1 influences the response of chondrocytes cultured in agarose constructs to IL-1β and dynamic compression. *Inflamm. Res.* **57**, 306-313 (2008).

44. R. J. Nims *et al.*, Continuum theory of fibrous tissue damage mechanics using bond kinetics: application to cartilage tissue engineering. *Interface Focus* **6**, 20150063 (2016).

45. N. O. Chahine, F. H. Chen, C. T. Hung, G. A. Ateshian, Direct measurement of osmotic pressure of glycosaminoglycan solutions by membrane osmometry at room temperature. *Biophys. J.* **89**, 1543-1550 (2005).

46. A. L. McNulty, N. E. Rothfusz, H. A. Leddy, F. Guilak, Synovial fluid concentrations and relative potency of interleukin-1 alpha and beta in cartilage and meniscus degradation. *J. Orthop. Res.* **31**, 1039-1045 (2013).

47. H. A. Leddy, A. L. McNulty, F. Guilak, W. Liedtke, Unraveling the mechanism by which TRPV4 mutations cause skeletal dysplasias. *Rare Dis* **2**, e962971 (2014).

48. S. Heller, R. O'Neil, *Molecular Mechanisms of TRPV4 Gating.* W. Liedtke, S. Heller, Eds., TRP Ion Channel Function in Sensory Transduction and Cellular Signaling Cascades. (CRC Press/Taylor & Francis, Boca Raton (FL), 2007).

49. C. J. O'Conor *et al.*, Cartilage-specific knockout of the mechanosensory ion channel TRPV4 decreases age-related osteoarthritis. *Sci. Rep.* **6**, 29053 (2016).

50. L. Ye *et al.*, TRPV4 is a regulator of adipose oxidative metabolism, inflammation, and energy homeostasis. *Cell* **151**, 96-110 (2012).

51. S. Wu, D. Fadoju, G. Rezvani, F. De Luca, Stimulatory effects of insulin-like growth factor-I on growth plate chondrogenesis are mediated by nuclear factor-κB p65. *J. Biol. Chem.* **283**, 34037-34044 (2008).

52. S. Wu, J. K. Flint, G. Rezvani, F. De Luca, Nuclear factor-κB p65 facilitates longitudinal bone growth by inducing growth plate chondrocyte proliferation and differentiation and by preventing apoptosis. *J. Biol. Chem.* **282**, 33698-33706 (2007).

53. I. Cambré *et al.*, Mechanical strain determines the site-specific localization of inflammation and tissue damage in arthritis. *Nature communications* **9**, 4613 (2018).

54. C. J. O'Conor, H. A. Leddy, H. C. Benefield, W. B. Liedtke, F. Guilak, TRPV4-mediated mechanotransduction regulates the metabolic response of chondrocytes to dynamic loading. *Proc. Natl. Acad. Sci. U. S. A.* **111**, 1316-1321 (2014).

55. W. R. Trickey, F. P. Baaijens, T. A. Laursen, L. G. Alexopoulos, F. Guilak, Determination of the Poisson's ratio of the cell: recovery properties of chondrocytes after release from complete micropipette aspiration. *J. Biomech.* **39**, 78-87 (2006).

56. J. C. Hou, S. A. Maas, J. A. Weiss, G. A. Ateshian, Finite Element Formulation of Multiphasic Shell Elements for Cell Mechanics Analyses in FEBio. *J. Biomech. Eng.*, (2018).

57. C. H. Hou, J. Huang, R. L. Qian, Identification of α NF-κB site in the negative regulatory element (ε-NRAII) of human ε-globin gene and its binding protein NF-κ B p50 in the nuclei of K562 cells. *Cell Res.* **12**, 79-82 (2002).

58. M. Nourbakhsh, K. Hoffmann, H. Hauser, Interferon- beta promoters contain a DNA element that acts as a position- independent silencer on the NF- kappa B site. *The EMBO journal* **12**, 451-459 (1993).

59. D. G. Gibson *et al.*, Enzymatic assembly of DNA molecules up to several hundred kilobases. *Nature methods* **6**, 343-345 (2009).

60. P. Salmon, D. Trono, Production and titration of lentiviral vectors. *Current protocols in human genetics* **54**, 12.10. 11-12.10. 24 (2007).

61. R. W. Farndale, D. J. Buttle, A. J. Barrett, Improved quantitation and discrimination of sulphated glycosaminoglycans by use of dimethylmethylene blue. *Biochim. Biophys. Acta* **883**, 173-177 (1986).

Acknowledgements

This work was supported by the NIH (AR76665, AG46927, AG15768, AR74240, AR73752, AR074992), Nancy Taylor Foundation, Arthritis Foundation, NSF EAGER Award, NSF Graduate Research Fellowship Program (DGE-1745038), and the Phillip and Sima Needleman Fellowship, the Duke School of Medicine, and a Duke Clinical and Translational Science Award (CTSA) UL1TR001117. We also thank Dr. Jonathan Brunger for his contribution in the design of the NF-κ−Br-circuits, Holly Dressman of the Duke Microarray facility, Isaura Rigo and Dawn Chasse for technical assistance, and Geoffrey Erickson, Scott Pritchard, and Remco Minkhorst for contributions to the cell mechanics assays.

Author Contributions

R.J.N, L.P., and F.G. conceived the project. R.J.N, L.P., N.B.H., A.S., A.K.R., C.J.O., B.Z., A.L.M., and F.G. designed the experiments. R.J.N and A.S. conducted the chondrocyte mechanical modulation experiments and the finite element modeling. N.B.O., C.J.O., W.B.L., B.Z, and A.L.M. planned, collected, and analyzed the microarray data of TRPV4 stimulation. R.J.N., L.P., J.L., S.S., J.K., and A.K.R. conducted mechanogenetic circuit experiments and analysis. R.J.N., L.P., and F.G. wrote the manuscript. All authors read, edited, and approved the final manuscript.

Data Availability

The microarray data generated and analyzed are available and are being submitted to the GEO repository. We will update this section to include the accession number once completed. Any other data are available from the corresponding author upon reasonable request.

Figures

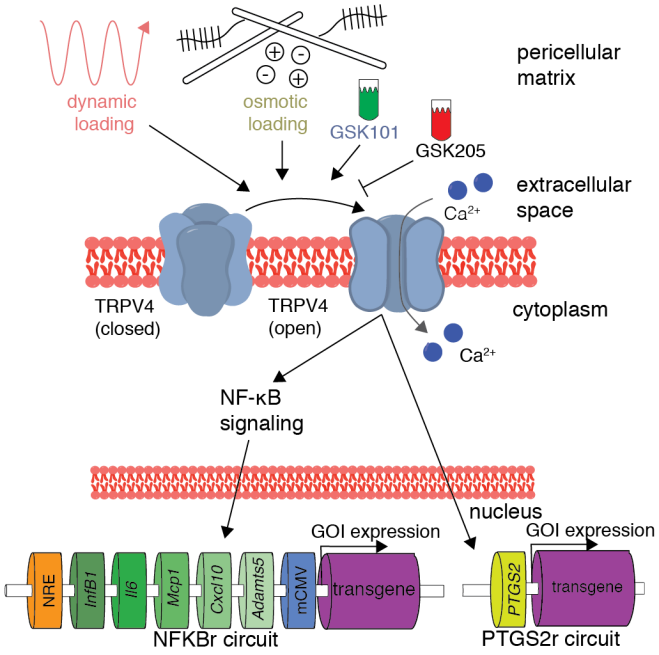

Fig. 1. Mechanogenetic transduction and therapeutic drug delivery approach. Transient receptor potential vanilloid 4 (TRPV4) is an osmotically-sensitive cation channel in the cell membrane of chondrocytes, which can be activated by mechanical loading secondary to mechano-osmotic coupling through the extracellular matrix or pharmacologically with the agonist GSK101. TRPV4 can also be inhibited with the antagonist GSK205. Upon TRPV4 activation, chondrocytes respond with intracellular calcium signaling that initiates NF-κB signaling and upregulation of the *PTGS2* gene. By lentivirally transducing synthetic mechanogenetic circuits that respond to either NF-κB activation or *PTGS2* upregulation into chondrocytes within an engineered cartilage tissue, mechanically activated TRPV4 signaling was used to drive transgene production of either a luciferase reporter or the therapeutic anti-inflammatory biologic interleukin-1 receptor antagonist (IL-1Ra).

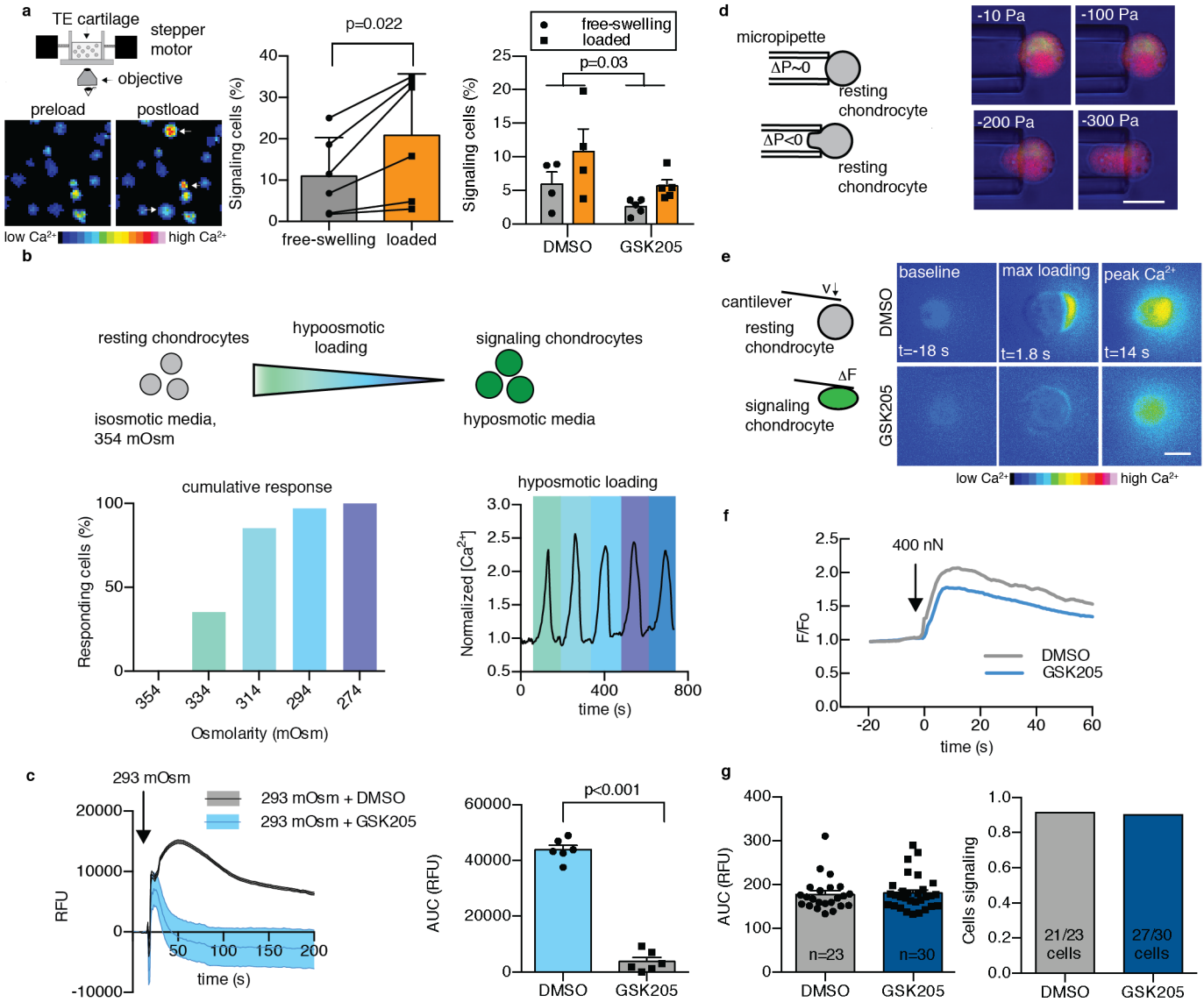

Fig. 2. Mechanical responsiveness of chondrocytes is mediated by hyposmotic stimulation of TRPV4. (a) Set-up of real-time cellular imaging tests of compressive mechanical loading. Loading chondrocytes within tissue engineered cartilage construct causes an increase in intracellular calcium compared to free swelling tissues constructs. Arrows indicate immediately-responsive cells. Scale bar is 50 µm. The number of cells exhibiting intracellular calcium signaling was increased by 108% after loading, and the TRPV4 antagonist GSK205 suppressed cellular calcium signaling (n=4-5 constructs per treatment). (b) Isolated chondrocytes are sensitive to osmotic perturbations and exhibit intracellular calcium increases in response to hyposmotic stimulation over a range of physiologic osmolarities (n=15-20 cells per group). (c) Chondrocyte responsiveness to hyposmotic stimulation is inhibited with the TRPV4 antagonist GSK205 (n=6 per treatment). (d) Chondrocytes are not sensitive to direct membrane stretch within the physiologic range of strains, as applied under isosmotic, isovolumetric conditions with micropipette aspiration (n=38, scale bar is 10 µm). (e) Direct cellular compression to high strains via a 400 nN load with an atomic force microscope induces intracellular calcium signaling. Scale bar is 10 µm. (f) Time-course analysis reveals GSK205 does not modulate calcium response of

chondrocytes to AFM loading. (g) TRPV4 inhibition alters neither the intensity of calcium responsiveness nor the population response to AFM compression (n=23-30 cells per group). Data are presented as mean ± SEM.

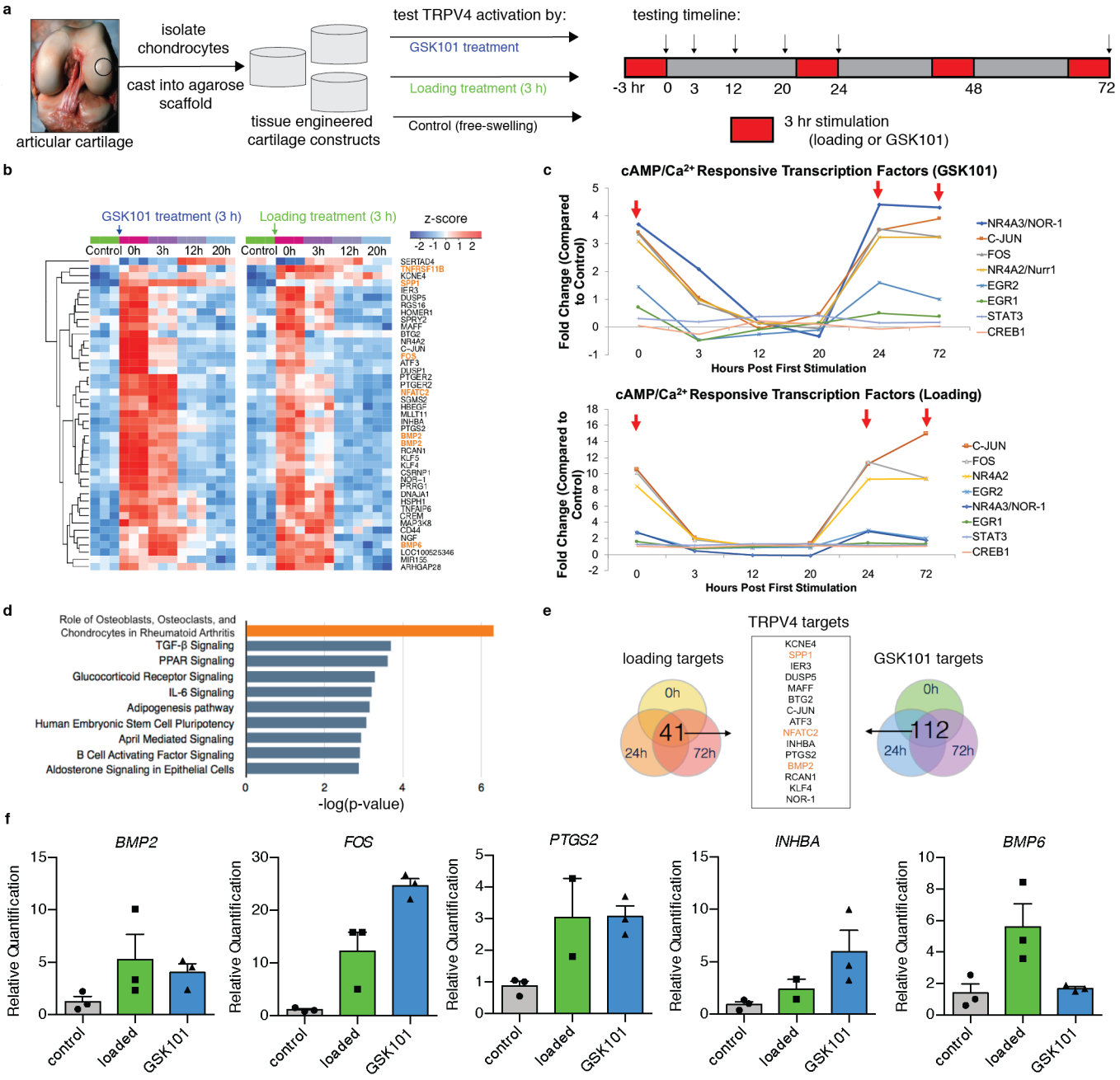

Fig. 3. Transcriptomic profile induced by TRPV4 activation. (a) Engineered cartilage tissue constructs were made from isolated primary porcine chondrocytes cast into agarose hydrogels. Tissue constructs were cultured in nutrient-rich media before deformational mechanical loading or GSK101 pharmacologic stimulation (red, 3 h/round) following the indicated time course and cartilage construct harvest (arrows). (b) 41 genes were differentially upregulated in response to TRPV4 activation and levels returned back to baseline after 12-20 h post loading (n=3/treatment/timepoint). (c) cAMP and calcium-responsive transcription factors were immediately and highly regulated by both mechanical loading and GSK101 stimulation (red arrows indicate removal from loading). (d) Pathway analysis based on transcription activity suggests both inflammatory and anabolic pathways are strongly regulated by TRPV4 activation. (e) Analysis of gene targets response after all bouts of mechanical loading and all bouts of GSK101 stimulation produces a list of distinctly-TRPV4 sensitive genes. (f) TRPV4-responsive targets from the microarray analysis were confirmed by qPCR (n=2-3).

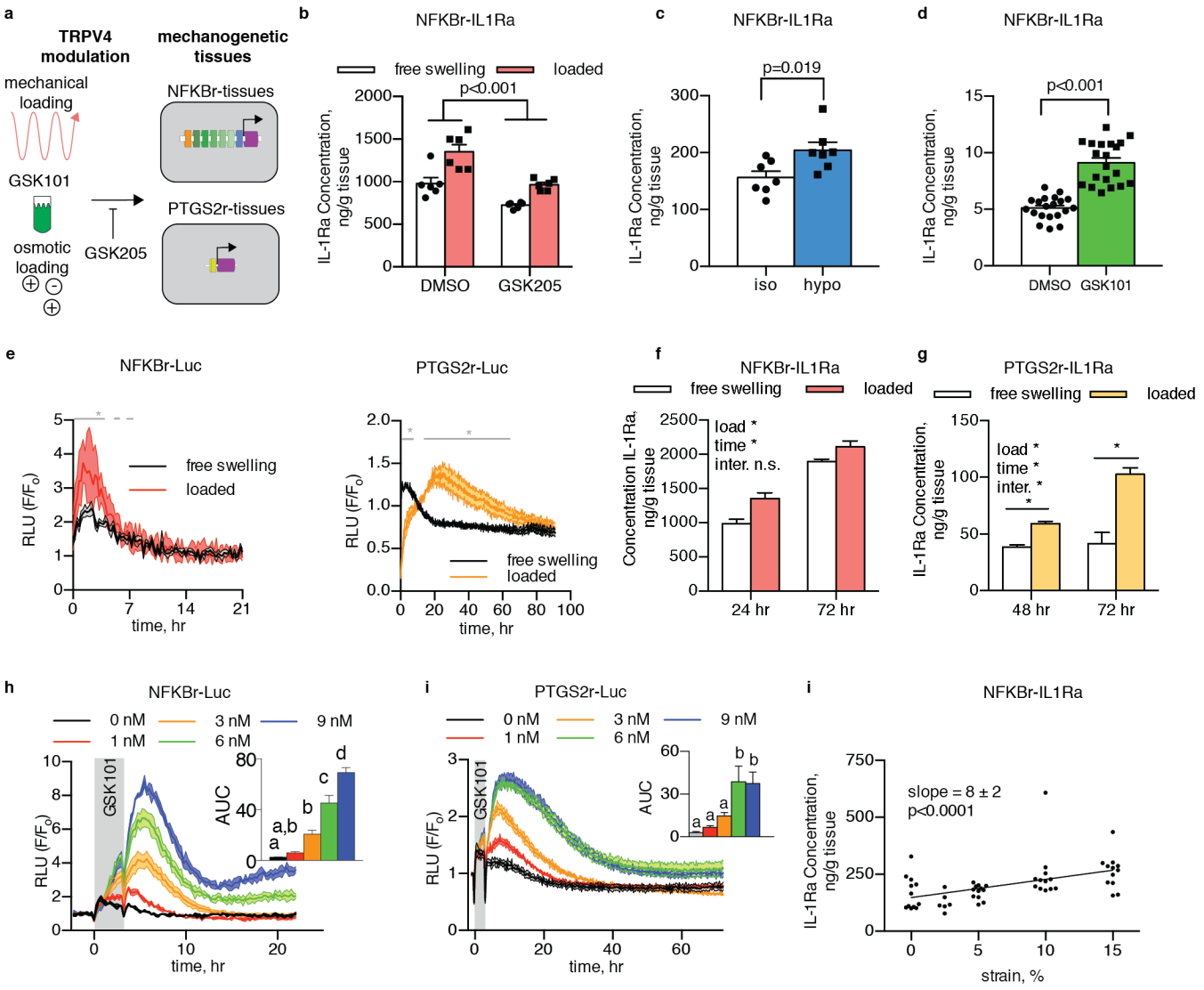

Fig. 4. Mechanogenetic cartilage tissue constructs respond to TRPV4 activation with dose-dependent sensitivity. (a) Mechanogenetic cartilage tissue constructs were tested with the TRPV4 activation mechanisms of mechanical loading, osmotic loading, and GSK101 pharmacologic stimulation and GSK205 was used to inhibit TRPV4 activation. (b) NFKBr-IL1Ra mechanogenetic engineered cartilage constructs respond to mechanical loading to increase IL-1Ra production ($p<0.001$), demonstrating circuit activation in response to loading. IL-1Ra is reduced with the addition of the TRPV4 antagonist GSK205, demonstrating TRPV4 activity controls the mechanogenetic circuits ($p<0.001$, n=6 per treatment). (c) NFKBr-IL1Ra mechanogenetic engineered cartilage constructs exposed to a step change in hyposmotic media produce more IL-1Ra than tissues exposed to a step change to isosmotic media, demonstrating circuit activation through osmotic stimulation ($p=0.019$, n=7 per group). (d) NFKBr-IL1Ra mechanogenetic engineered cartilage exposed to 3 h d^{-1} stimulation of GSK101 produce more IL-1Ra than vehicle controls ($p<0.001$, n=20 per group). (e) After mechanical loading, NFKBr-Luc mechanogenetic cartilage tissue constructs quickly activate and inactivate as measured by bioluminescent imaging, while PTGS2r-Luc tissue constructs take longer to peak and remain at levels higher than baseline, free-swelling tissues, for longer (gray asterisked line denotes $p<0.05$ between free-swelling and loaded tissues,

n=3-6 per group). (f) NFKBr-IL1Ra tissues respond to loading after 24 h and 72 h, indicating differential expression occurs in the first 24 h. (g) PTGS2r-Luc mechanogenetic tissues continue to increase IL-1Ra production even after 72 h post-loading, evident by increasing IL-1Ra in loaded tissues. (h) NFKBr-Luc tissues respond with dose-dependent activation to different levels of GSK101 stimulation through 9 nM GSK101 (letters denote significant differences, $p<0.05$, n=2-4 per group). (i) PTGS2r-Luc tissues are sensitive to TRPV4 activation up to 6 nM GSK101 (letters denote significant differences, $p<0.05$, n=2-4 per group). (j) NFKBr-IL1Ra tissues respond in a dose-dependent manner to mechanical loading from 0 to 15 % compressive sinusoidal strain for 3 h ($p<0.001$, n=5-12). Data are presented as mean ± SEM.

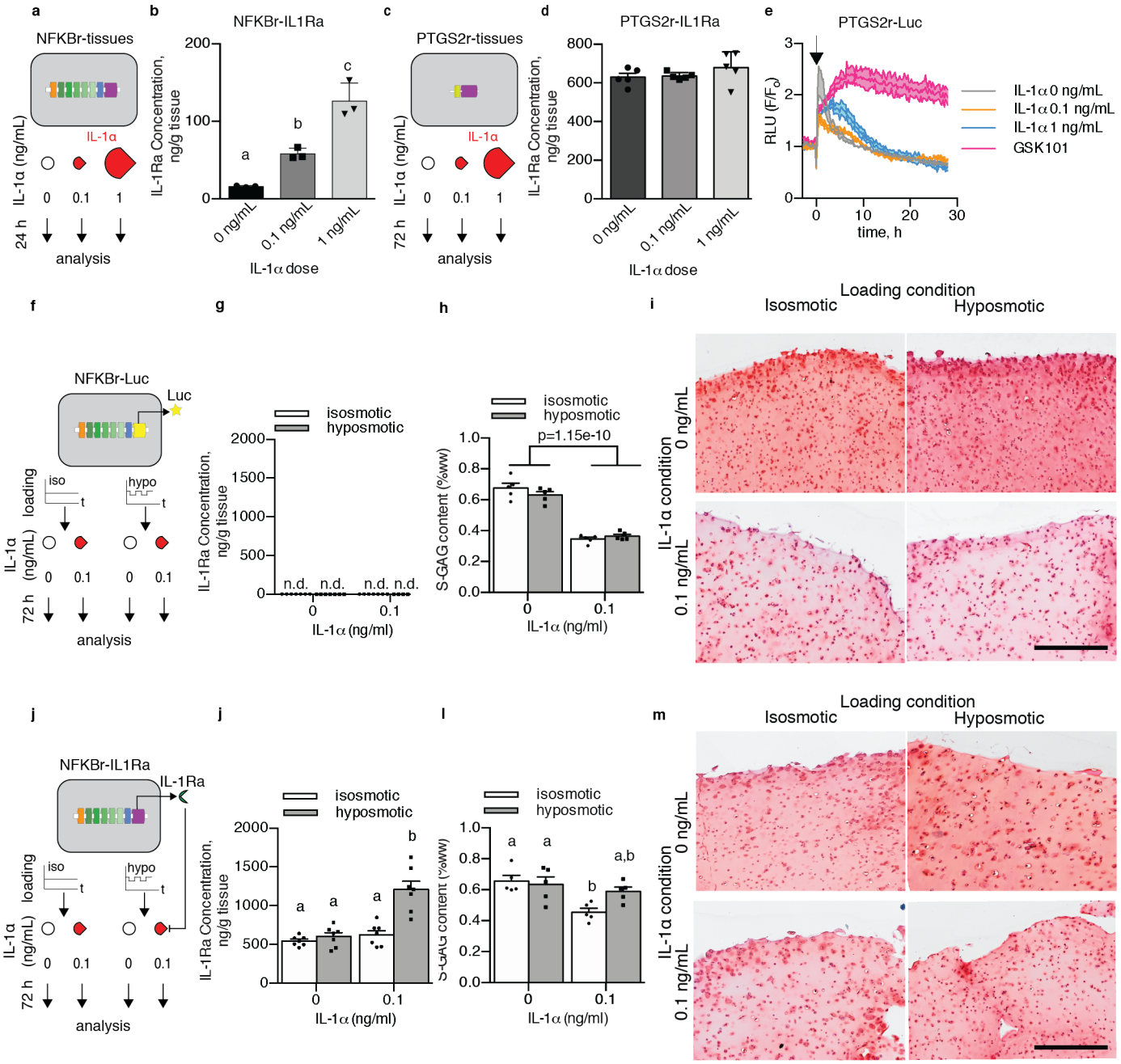

Fig. 5. Loading of mechanogenetic cartilage tissue constructs protects constructs against inflammatory IL-1α. (a) The inflammatory response of NFKBr-IL1Ra mechanogenetic tissue constructs was tested by supplementing IL-1α in the media. (b) NFKBr-IL1Ra tissues produce IL-1Ra in response to IL-1α in a dose-dependent manner at 0.1 ng/mL and 1 ng/mL (n=3 per dose, $p<0.001$). (c) The inflammatory response of PTGS2r-mechanogenetic tissues was tested by supplementing IL-1α in the media. (d) PTGS2r-IL1Ra tissues do not differentially respond to IL-1α between 0 and 1 ng/mL doses (n=5 per dose). (e) PTGS2r-Luc mechanogenetic tissues are not differentially altered in circuit activity to chronic IL-1α, while chronic GSK101 increases circuit activation (n=2 per condition, arrow indicates onset of stimulation). (f) To test the mechano-inflammatory response of mechanogenetic tissues, osmotic loading (3 h d^{-1}) and IL-1α inflammatory challenge (0 or 0.1 ng/mL) were applied to NFKBr-Luc tissue constructs over the course of 72 h. (g)

NFKBr-Luc tissues do not produce any measurable anti-inflammatory IL-1Ra (n=7 per group). (h) NFKBr-Luc tissues lost S-GAG content in the presence of IL-1α and osmotic loading did not mediate this response (n=5 per group). (i) Histology demonstrated loss of safranin-O in IL-1α cultured tissues. (j) To test the mechano-inflammatory response of mechanogenetic tissues, osmotic loading (3 h d^{-1}) and IL-1α inflammatory challenge (0 or 0.1 ng/mL) were applied to NFKBr-IL1Ra tissues over the course of 72 h. (j) IL-1Ra levels were increased in the presence of both inflammation and loading over inflammation alone (n=7 per group, $p<0.001$). (l) S-GAG content in NFKBr-IL1Ra tissue constructs incubated under IL-1α inflammatory challenge (0 or 0.1 ng/mL) and/or osmotic loading (different letters denote significant differences, $p<0.05$, n=5 per group). (m) NFKBr-IL1Ra mechanogenetic tissues displayed similar levels of safranin-O staining when not cultured in the presence of IL-1α, while 3 d IL-1α incubation reduced safranin-O staining in isosmotic tissues but not hyposmotic tissues. Data are presented as mean ± SEM.

Supplemental Tables and Figures

Supplementary Table 1. Tabulated values of all differentially expressed genes over the first 24 h cycle after initial GSK101 stimulation taken at 0, 3, 12, and 20 h after the cessation of stimulation.

Supplementary Table 2. Tabulated values of all differentially expressed genes over the first 24 h cycle after initial mechanical loading stimulation taken at 0, 3, 12, and 20 h after the cessation of stimulation.

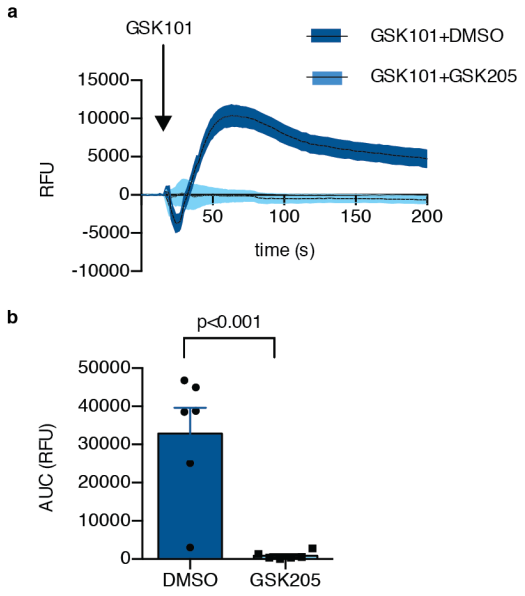

Fig. S1. The TRPV4 agonist GSK101 stimulated intracellular calcium signaling immediately after addition (top) and this signaling was potently abolished by the antagonist GSK205. (a) Calcium signaling temporal dynamics of GSK101 activation. (b) Cumulative area-under-curve (AUC) of the temporal data ($p<0.001$, $n=6$).

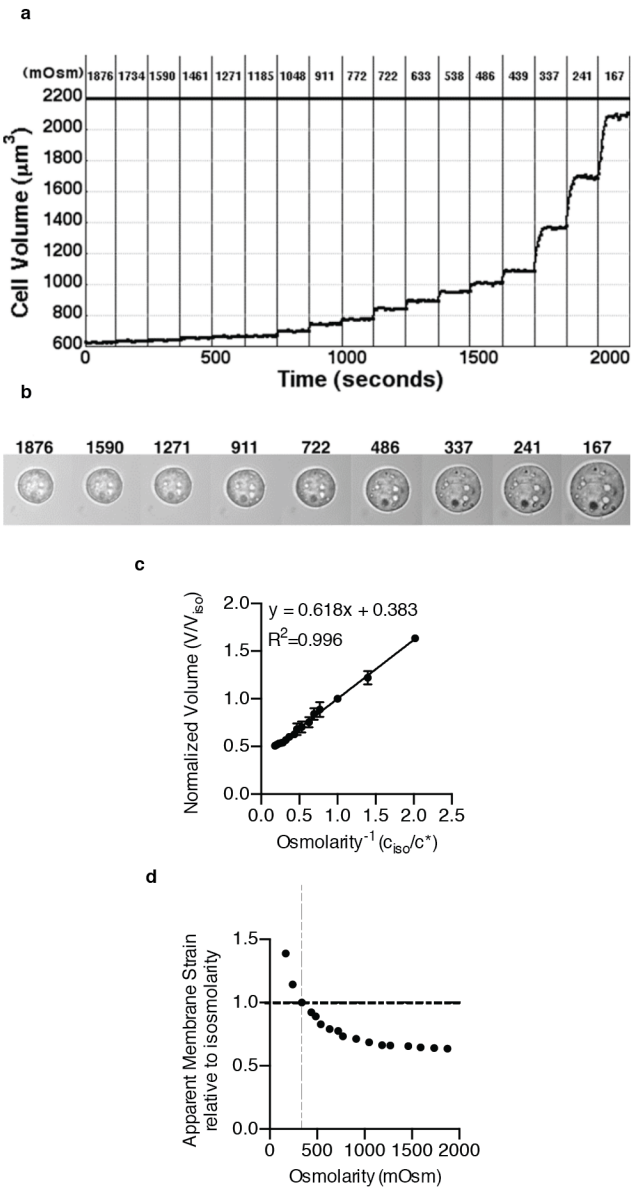

Fig. S2. (a) Chondrocytes respond mechanically to changes in external osmolarity through a wide range of osmolarities as measured by (b) DIC images from isolated chondrocytes undergoing osmotic loading. (c) Chondrocytes behave as ideal osmometers to changes osmolarity as displayed on a Ponders plot which plots the normalized inverse osmolarity to the normalized cell volume. The slope of the line (0.618) corresponds to the volume fraction that is osmotically-active within the chondrocyte (n=18 cells). (d) Figure in (c) converted to demonstrate non-linear influence on apparent membrane strain resulting from osmotic fluctuations.

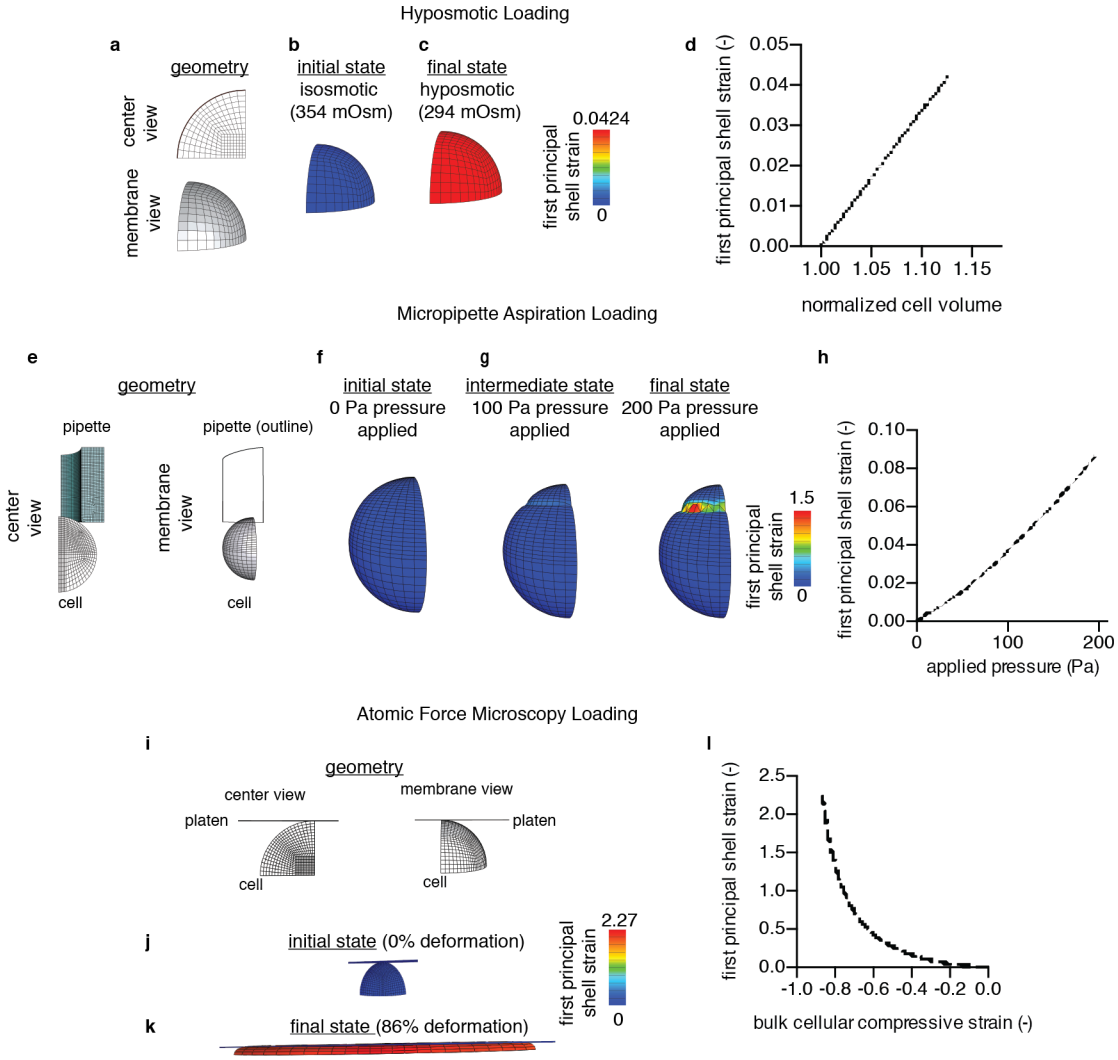

Fig. S3. Finite element models of cellular loading conditions: hyposmotic (a-d), micropipette aspiration (e-h), and direct AFM loading (i-l). Models are run of an octant or quadrant cell by employing appropriate axisymmetry boundary conditions. Simulation figures represent the original geometry (a, e, i, center and membrane views), the pre-strained membrane state (b, f, j), and the deformed states (c, g, k). For osmotic loading, a hyposmotic step of -60 mOsm was applied; for micropipette aspiration 100 and 200 Pa pressures were applied; for AFM compression a 86% cell deformation was applied. Scale bar depicts the first principle strain of the cell membrane. Plots (d, h, l) represent the relationship between the applied deformation method and the first principal membrane strain; the micropipette plotted relationship is shown for a membrane element residing within the pipette and the AFM plotted relationship is shown for a membrane element residing along the equatorial (peak) region of membrane strain.

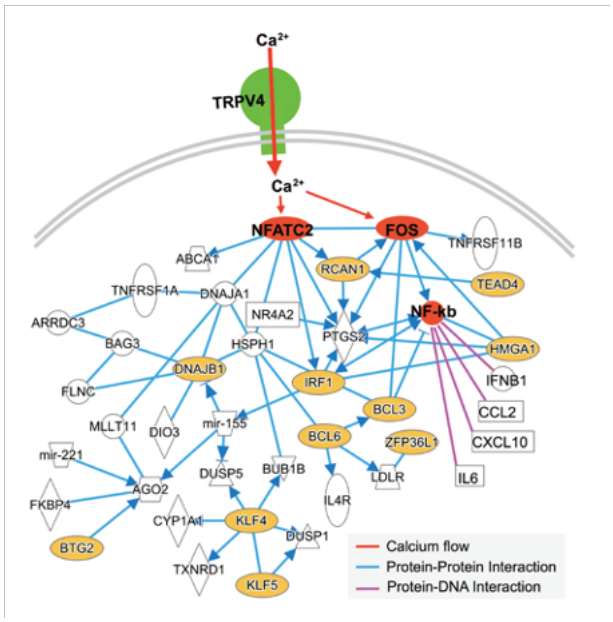

Fig. S4. Network schematic for intracellular pathways stimulated by TRPV4 activation.

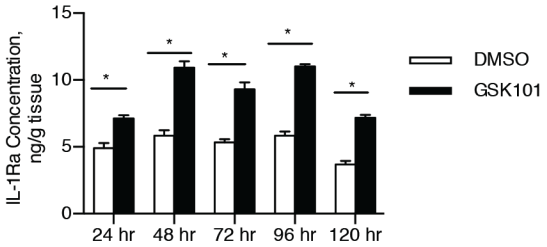

Fig. S5. Daily IL-1Ra production from NKFBr-IL1Ra mechanogenetic cartilage exposed to either 1 nM GSK101 or vehicle (DMSO) constructs for 3 h d^{-1} every 21 h. Data are pooled and presented cumulatively in Fig. 4c. n=4 per group/timepoint, * denotes $p<0.05$ between GSK101 and vehicle compared on each day.

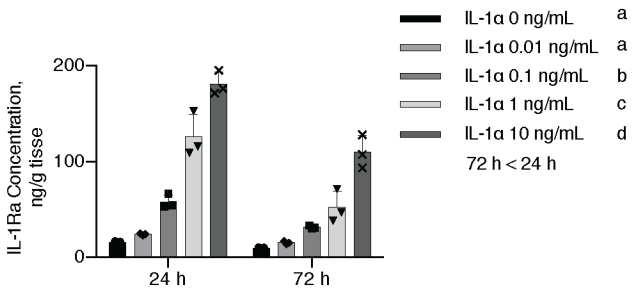

Fig. S6. NFKBr-IL1Ra engineered cartilage responds in a dose-dependent manner to IL-1α robustly for extended durations (24 and 72 h of exposure). Subset data from 24 h exposure depicted in Fig. 5A. Different letters depict significant differences in groups.

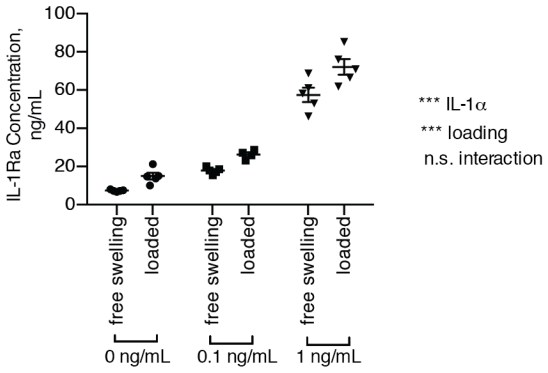

Fig. S7. NFKBr-IL1Ra mechanogenetic tissues respond to both IL-1α and deformational mechanical loading at 24 h in a coculture system with graded IL-1α conditions (interaction n.s., $p>0.05$; *** denotes $p<0.05$).

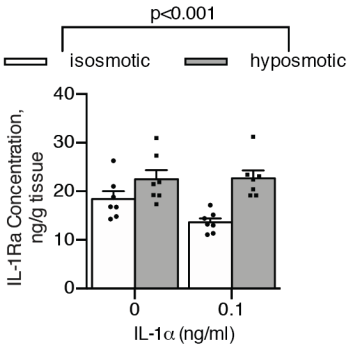

Fig. S8. Isosmotic (control) and hyposmotic (loaded) treatments of PTGS2r-IL1Ra constructs in the presence of 0 or 0.1 ng/mL IL-1α in a coculture setting responded only to the loading factor produced a significant difference in IL-1Ra production response ($p<0.001$). Data are presented as mean ± SEM.